Article

Dynamics and Interaction of Interleukin-4 Receptor Subunits in Living Cells

Hetvi Gandhi,[1] Remigiusz Worch,[1,2] Kristina Kurgonaite,[3] Martin Hintersteiner,[4] Petra Schwille,[1,5] Christian Bökel,[3] and Thomas Weidemann[1,5,*]

[1]BIOTEC/Biophysics, Technische Universität Dresden, Dresden, Germany; [2]Institute of Physics, Polish Academy of Sciences, Warsaw, Poland; [3]Center for Regenerative Therapies Dresden, Technische Universität Dresden, Dresden, Germany; [4]Novartis Institutes for BioMedical Research, Basel, Switzerland; and [5]Max Planck Institute of Biochemistry, Am Klopferspitz 18, 82152 Martinsried, Germany

ABSTRACT It has long been established that dimerization of Interleukin-4 receptor (IL-4R) subunits is a pivotal step for JAK/STAT signal transduction. However, ligand-induced complex formation at the surface of living cells has been challenging to observe. Here we report an experimental assay employing trisNTA dyes for orthogonal, external labeling of eGFP-tagged receptor constructs that allows the quantification of receptor heterodimerization by dual-color fluorescence cross-correlation spectroscopy. Fluorescence cross-correlation spectroscopy analysis at the plasma membrane shows that IL-4R subunit dimerization is indeed a strictly ligand-induced process. Under conditions of saturating cytokine occupancy, we determined intramembrane dissociation constants ($K_{d,2D}$) of 180 and 480 receptors per μm^2 for the type-2 complexes IL-4:IL-4Rα/IL-13Rα1 and IL-13:IL-13Rα1/IL-4Rα, respectively. For the lower affinity type-1 complex IL-4:IL-4Rα/IL-2Rγ, we estimated a $K_{d,2D}$ of ~1000 receptors per μm^2. The receptor densities required for effective dimerization thus exceed the typical, average expression levels by several orders of magnitude. In addition, we find that all three receptor subunits accumulate rapidly within a subpopulation of early sorting and recycling endosomes stably anchored just beneath the plasma membrane (cortical endosomes, CEs). The receptors, as well as labeled IL-4 and trisNTA ligands are specifically trafficked into CEs by a constitutive internalization mechanism. This may compensate for the inherent weak affinities that govern ligand-induced receptor dimerization at the plasma membrane. Consistently, activated receptors are also concentrated at the CEs. Our observations thus suggest that receptor trafficking may play an important role for the regulation of IL-4R-mediated JAK/STAT signaling.

INTRODUCTION

The interleukin-4 receptor (IL-4R) subunits are single-pass transmembrane proteins that belong to the important superfamily of hematopoietic cytokine receptors (1). Throughout this family, assembly of ternary ligand-receptor complexes along with conformational changes constitute a prerequisite for proximity-driven cross-activation of receptor-chain-associated, cytoplasmic Janus kinases (JAKs) (2,3). Despite this general scheme, the proposed conformational changes leading to receptor activation are surprisingly diverse (4–8).

Unlike homotypic receptors such as growth hormone or erythropoietin receptor that form transmembrane domain-mediated dimers, IL-4Rα and IL-2Rγ (common γ-chain, γ_c) diffuse as monomers in the plasma membrane (9). Thus, at least for the heterotypic receptor types, a diffusion-controlled recruitment of the second receptor chain can be assumed to trigger JAK activation and signal transduction at the plasma membrane. In addition, the IL-2Rγ subunit is shared between different cytokine receptor complexes (10), and the local dynamic equilibrium of complex formation may therefore determine the signaling output (11,12). However, for only a few of these family members, ligand-induced dimerization has been addressed at the molecular level in living cells (4,11,13,14).

IL-4R is a well-known example of such a heterotypic receptor. IL-4 specifically binds to the IL-4Rα chain, enabling it to recruit either IL-2Rγ to form a type-1 receptor complex or IL-13Rα1 to form a type-2 receptor complex. Alternatively, the type-2 receptor complex can be induced by IL-13 bound to IL-13Rα1 (15,16). Thus, the type-2 complex features a symmetrical configuration in the sense that both receptor subunits can serve either as ligand-presenting or recruited-receptor subunits.

The mutual interactions between ligands and receptor subunits have been characterized in great detail (17–19). To interfere with this signaling pathway, IL-4 antagonists were designed that could still bind the α-chain but were impaired in recruiting the second receptor subunit (17,20–22). A comprehensive set of crystal structures for the ectodomains of all three types of IL-4R complexes is now available (10,23,24). The affinities between the ligand bound and the recruited receptor ectodomains have been measured in free solution (24,25) and confirm the cellular observations that ligand affinity is significantly biased toward one of the receptor subunits (8). However, when embedded in the plasma

Submitted March 4, 2014, and accepted for publication July 24, 2014.

*Correspondence: weidemann@biochem.mpg.de

Martin Hintersteiner's current address is Bioseutica Group, Corso Elvezia 4, 6900 Lugano, Switzerland.

Hetvi Gandhi's current address is Imagine, Institut Des Maladies Génétique, Boulevard de Montparnasse 24, 75015 Paris, France.

Editor: Susan Pierce.

0006-3495/14/12/2515/13 $2.00

http://dx.doi.org/10.1016/j.bpj.2014.07.077

membrane of a living cell complex, processes such as endocytosis or raft partitioning come into play that may influence receptor complex assembly (4,26–28).

Using fluorescently labeled IL-4, we previously observed by fluorescence cross-correlation spectroscopy (FCCS) that the IL-13Rα1 chain is recruited into a complex, whereas IL-2Rγ containing type-1 dimers could not be detected in the plasma membrane of HEK293T cells (11). Using synthetic dyes for external receptors labeling in combination with native ligands, we can now detect ligand-induced dimerization for all three IL-4R complexes. Employing a truncated, dominant negative mutant of the IL-4Rα chain even provides sufficient accuracy to quantify for the first time, to our knowledge, two-dimensional dissociation constants in the plasma membrane plane. The affinities are surprisingly weak, pointing toward a cellular concentration mechanism that is necessary to drive dimerization and a stable receptor activation. Based on various additional approaches, we propose that constitutive endocytosis into a novel subpopulation of early endosomes (cortical endosomes, CEs) fulfills this role. These results therefore provide important and unexpected mechanistic insight into IL-4R-mediated JAK/STAT signaling.

MATERIALS AND METHODS

Molecular biology and cloning

Molecular cloning was performed as described in Worch et al. (9) and Weidemann et al. (11). Plasmids encoding for mRFP-Rab5 (29) and mRFP-Rab7 (30) are described. mCherry-Rab11 was donated by M. Zerial (MPI-CBG, Dresden, Germany).

pJAK3-tagRFP was created from pJAK3-eGFP (31) by replacing eGFP (*Age*I/*Not*I) by tagRFP (NCBI; GI:187373120). pNHis-IL2Rg-N2 was derived from pNHis-IL2Rg-eGFP-N2 (9) by GFP excision (*Not*I/*Sma*I) and fill-in. pCMV-STAT6 was generated by replacing the eGFP in pEGFP-N1 with the ORF of human STAT6 (F1KB4980; Kazusa DNA Research Institute, Kisarazu, Chiba, Japan).

mRNA of HEK293T cells was extracted as described in Weidemann et al. (11). Q-PCR was performed on a Lightcycler 480 (Roche, Penzberg, Germany) in 96-well microplates (Biozym, Hessisch Oldendorf, Germany). Primer and plasmid sequences are available upon request.

Cell culture, reporter gene assay, and immunoblotting

HEK293T cells were cultured as described in Weidemann et al. (11). For the reporter gene assay HEK293T, cells were seeded in a 96-multiwell plate and transfected at 30–40% confluence with 50 ng p3xSTAT6-RE-Luc (STAT6 responsive firefly luciferase), 25 ng pRLTK (constitutive Renilla luciferase), and up to 125 ng of plasmids coding for combinations of IL-4R subunits and STAT6. After 24 h, cells were stimulated with IL-4 or IL-13 (10–20 ng/mL) for 12 h. Before experiment, the cells were washed twice with ice-cold PBS, lysed, and transferred into a white 96-well plate (Corning Inc., Corning, New York). For detection we used luminescent chemicals (Stop&Glo; Promega, Madison, WI) and a Glomax plate reader (Promega). All data points were measured in triplicates.

For immunoblotting, cells were stimulated with IL-4 or IL-13 (Gibco, Grand Island, NY) at 37°C for 30 min, washed with ice-cold PBS (phosphate-buffered saline), and lysed (25 mM Tris pH 7.2, 150 mM NaCl, 5 mM $MgCl_2$, 0.2% NP-40, 1 mM DTT) with 5% Glycerol and the Complete Protease Inhibitor cocktail (Roche). Proteins were detected after blotting with phospho-STAT6 (mouse, 1:2000; Santa Cruz Biotechnology, Dallas, TX) or GAPDH (mouse, 1:4000; Santa Cruz Biotechnology) and visualized with HRP-coupled goat anti-mouse (1:4000; Sigma, St. Louis, MO) using ECL+ (Life Technologies, Norwalk, CT). The STAT6 response kinetics was fitted with a logistic function using the software ORIGIN (OriginLab, Northampton, MA),

$$[\mathrm{pSTAT6}] = A2 + \frac{A1 - A2}{1 + (t/t_0)^p}, \tag{1}$$

with t_0 as a typical time constant (half-maximum activation) and $A1$, $A2$, and p as parameters.

Synthesis of trisNTA dyes

Synthesis of the trisNTA probe was achieved by coupling of three carboxy functionalized NTA moieties, prepared by alkylation of the amino function of a protected glutamate derivative, to three amino groups of a cyclam scaffold (32,33). An N-Boc protected 6-amino caproic acid spacer was attached to the fourth amino group. After deprotection, the primary amine of the spacer was conjugated to amino-reactive dyes (QSY-7 (Alexa647, 5-carboxytetramethylrhodamine); Life Technologies). The Ni^{2+} saturated compounds were purified by HPLC using aqueous 400 mg/L ammonium acetate/acetonitrile gradients and characterized by electrospray ionization-mass spectrometry.

Imaging and immunocytochemistry

Cells were either imaged live (11) or after fixing, as described in Michel et al. (34). Primary antibodies: EEA1 (mouse, 1:500; Abcam, Cambridge, UK), phospho-Y497-IL-4Rα (rabbit, 1:1000; Abcam), and Lamp1 (mouse; 1:300; Santa Cruz Biotechnology). Live cell imaging was done at 22°C in air buffer (150 mM NaCl, 20 mM HEPES pH 7.4, 15 mM glucose, 46 mM trehalose, 5.4 mM KCl, 0.85 mM $MgSO_4$, 1.7 mM $CaCl_2$, 0.15 mg/mL bovine serum albumin).

Fluorescence recovery after photobleaching (FRAP)

Experiments were performed at 22°C, on an LSM780 (Zeiss, Jena, Germany) with a 40×, NA 1.2 objective using a multichannel GaAsP detector to collect eGFP emission (490–560 nm). HEK293T cells transiently expressing IL-2Rγ/JAK3-eGFP complexes were analyzed in 8-well chambered Labtek slides (Nalge Nunc, Roskilde, Denmark). The regions of interest (ROIs) were defined perpendicular to the membrane plane (2.5 × 2.5 μm^2) (35). JAK3-eGFP was bleached to ~20% before recovery using the combined excitation of the 405-nm and 488-nm laser lines. We recorded 50–100 frames over a period of 5–10 min. Excitation-induced bleaching in the ROI (area A) during the postbleach period was corrected by a distant, nonbleached control ROI (area B). The intensity curves were corrected for imaging-dependent bleaching, denoting B_0 as the prebleach intensity in area B (36),

$$C(t) = \frac{A(t)}{B(t)/B_0}. \tag{2}$$

Then we normalized the signal to initial prebleach intensity level A_0 and C_1, the first time-point of the corrected postbleach series

$$D(t) = \frac{C(t) - C_1}{A_0 - C_1}. \tag{3}$$

Finally, to derive the time constants t_0, $D(t)$ was fitted with a saturating exponential

$$y(t) = k\left(1 - e^{-t/t_0}\right). \quad (4)$$

Stimulated emission depletion (STED) microscopy

Superresolution imaging of JAK3-eYFP positive endosomes was performed on a TCS SP5 confocal microscope (Leica Microsystems, Wetzlar, Germany). eYFP was excited at 514 nm, and excitation depletion was achieved with a 592-nm laser (Leica Microsystems) delivering an ~350 mW at the object plane. Images were acquired with a 100×, NA = 1.4 oil lens (STED orange, Leica Microsystems). Pixel size for STED imaging was set to 32 nm, resulting in a 2–3-fold oversampling.

Total internal reflection fluorescence (TIRF) microscopy

For time-lapse microscopy, the cells were imaged with a Life Cell AF6000 LX (Leica Microsystems) TIRF microscope equipped with a 37°C incubation chamber. Imaging was done with a HCX PL Apo 100× NA 1.46 oil objective, a QAX filter set for separate excitation and emission of eGFP and A647, and a cooled, high sensitivity electron-multiplying charge-coupled device camera (Andor Technology, Belfast, UK). Time series were taken with an electron-multiplying gain of 300 V and a frame rate of 500 ms.

FCCS

Technically, FCCS measurements and data analysis were performed as described in Weidemann et al. (11). However, trisNTA-A647 was used as an external label for the His-tagged IL-4Rα constructs. To minimize signal instabilities, the focal volume was placed in a homogeneous area of the bottom membrane, close to the glass support. Measurements were taken at 22°C with excitation intensities resulting in 2–3 kHz per particle in the A647 channel and 2–4 kHz per particle in the eGFP channel. For K_d determination, see the Appendix. Fitting was performed with the open-source software PyCorrFit (37).

Quantitative APD imaging

Receptor trafficking into JAK3-eGFP positive endosomes was measured by the uptake of preloaded external dye trisNTA-A647 in cells expressing His-tagged receptor subunits. Cells were seeded and transfected in 8-well Labtek chambers (Nunc). For IL-2Rγ kinetics, we used pNhis-IL2Rg-N2 (80 ng), pJAK3-eGFP (50 ng), and pIL4Ra-N1 (40 ng). For IL-4Rα kinetics, we used pIL2Rg-N1 (80 ng), pJAK3-eGFP (50 ng), and pNhis-IL4Ra-N1 (40 ng) in the absence or presence of 20 ng/mL IL-4 (Life Technologies). Twenty-four hours posttransfection, cells were washed twice with air buffer and chilled for 20 min on ice. Cells were then stained with 150 nM trisNTA-A647 in air buffer for 20 min on ice, washed once in air buffer, and transferred to 37°C starting endocytosis. At different time-points, cells were fixed in 4% PFA/PEM.

Confocal imaging was performed on a LSM780 (Zeiss) using avalanche photo-diode detectors. The 16-bit images were recorded with a 40×, NA 1.2 water immersion objective, using a 75-μm pinhole at a pixel dwell time of 50 μs using filter settings for eGFP (505–610 nm) and A647 (655 nm, long-pass). Laser powers were adjusted to stay <1 MHz. Each cell was imaged in three different planes at 1.5-μm distance. For image analysis, we manually identified cortical endosomes in the eGFP channel; an automated script then identified the maximum intensity and extracted the total counts of a centered 3×3 pixel bin (MATLAB, Rel. 2010a; The MathWorks, Natick, MA) in the A647 channel. Endosomes showing intensities exceeding the linear range were flagged and excluded. Average loading per cell (binning 50–100 endosomes) was used for statistical analysis. For fitting the average trafficking kinetics, we used a hyperbolic function (ORIGIN, OriginLab, Northampton, MA).

RESULTS

HEK293T cells as a model system for analyzing IL-4R-mediated signaling

We studied IL-4R subunit interactions in HEK293T cells that are amenable to imaging-based biophysical approaches due to their size and adherent growth. HEK293T cells endogenously express type-2 signaling components but not the type-1 components IL-2Rγ and JAK3 or STAT6 (Fig. 1 *A*). Because STAT6 phosphorylation and STAT6-dependent reporter gene assays provide a highly specific readout for IL-4R signaling output (16), we assayed pathway activation in HEK293T cells transiently expressing STAT6. Consistent with the endogenous presence of type-2 IL-4R subunits, STAT6 could be activated by both IL-4 and IL-13 (Fig. 1 *B*, and see Fig. S1 in the Supporting Material).

We tested the activity of the various ectopically expressed receptor constructs by a STAT6-responsive luciferase reporter gene assay (Fig. 1 *C*). HEK293T cells did not show IL-4-dependent STAT6 reporter activation in the absence of STAT6. Coexpression of full-length IL-4Rα chain increased the IL-4 response and the baseline. IL-4Rα cytoplasmic deletion constructs (IL-4Ram266 constructs comprised of the amino acids 1–266) lacking the STAT6 docking site dominantly suppressed the endogenous machinery, indicating trafficking behavior similar to that of the endogenous receptors. Their competitive potential was unaffected by N-terminal His-tags, C-terminal eGFP, or both. In contrast, luciferase expression after overexpression of the second receptor subunits IL-13Rα1 or the pair IL-2Rγ/JAK3 was comparable to stimulation of the endogenous type-2 receptors suggesting that the ligand binding α-chain is limiting. In both cases, the signal was suppressed by truncated tails. Although the overexpression of individual subunits therefore does not negatively interfere with signaling, the deletion constructs outcompete the endogenous type-2 machinery at comparable overexpression levels (Fig. 1 *C*, see also the FCCS quantifications below).

Ligand-induced IL-4R subunit recruitment at the cell surface

To probe surface-expressed receptors by FCCS, we first developed an external labeling procedure. Nonneutralizing external labels offer the possibility to compare cross-correlation amplitudes and hence dimerization levels in the absence and presence of unlabeled, and thus fully active, cytokine ligands. For labeling we synthesized hexahistidine

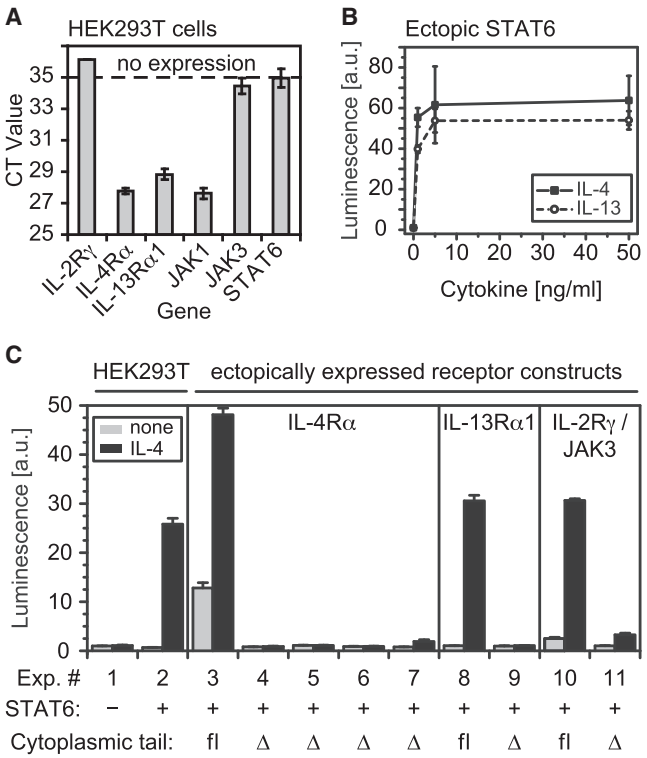

FIGURE 1 HEK293T as a model for IL-4R-mediated JAK/STAT signaling. (*A*) Q-PCR detects mRNA (low cycle-threshold value) for IL-4Rα, IL-13Rα1, and JAK1, but not for the type-1 receptor components IL-2Rγ and JAK3 or the transcription factor STAT6. (*B*) Dual-luciferase assay shows STAT6 responsive gene activation by both IL-4 and IL-13 in HEK293T cells transiently expressing STAT6. (*C*) Testing fluorescently tagged receptor constructs by dual-luciferase assay: IL-4-dependent reporter activation requires STAT6 (No. 1–2). Coexpression of full-length IL-4Rα chain increases the IL-4 response and the baseline (No. 3). Truncation of the IL-4Rα cytoplasmic tail (marked by Δ) dominantly suppresses the endogenous signaling (No. 4–7). N-terminal His-tags (Nos. 6 and 7) or C-terminal eGFP (Nos. 5 and 7) do not affect competitive ability. Overexpression of IL-13Rα1 or IL-2Rγ/JAK3 show little increase in signaling as compared to endogenous levels. In both cases the signal was suppressed by deletion constructs with truncated tails (Nos. 9 and 11). Constructs used: No. 2–11 STAT6, No. 3 IL4Ra-eGFP, No. 4 IL4Ram266, No. 5 IL4-Ram266-eGFP, No. 6 H6-IL4Ram266, No. 7 H6-IL4Ram266-eGFP, No. 8 IL13Ra1-eGFP, No. 9 IL13Ra1m356-eGFP, No. 10 H6-IL2Rg-eGFP/JAK3, and No. 11 IL2Rgm271/JAK3; *m* indicates the mature amino-acid number after which the receptor was truncated. Error bars indicate SD.

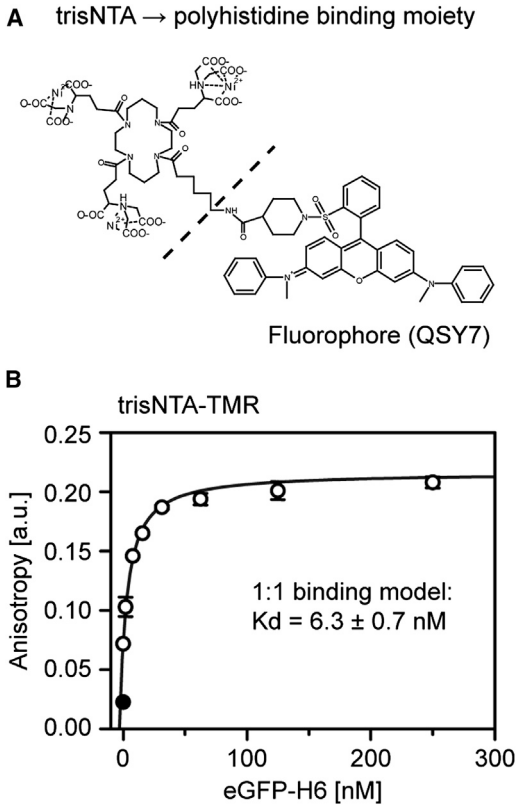

FIGURE 2 trisNTA-coupled fluorescent dyes bind reversibly to hexahistidine tags. (*A*) Chemical structure of trisNTA-QSY7. (*B*) Titration of purified eGFP genetically fused to a C-terminal His-tag. The increase in trisNTA-TMR fluorescence anisotropy reflects the degree of binding. The anisotropy of TMR (tetramethylrhodamine) alone is also shown (*solid circle*, triplicates ± SD).

binding dyes, which were introduced recently as a promising tool for receptor research (32,33). The bifunctional compounds consist of three nitrilotriacetic acid groups attached to a tetravalent, cyclic scaffold (trisNTA). A fourth substitution carries an aliphatic linker with an N-terminal amino group suitable for the conjugation of aminoreactive fluorescent dyes (Fig. 2 *A*). By this modular approach we produced TAMRA, QSY7, and Alexa647 (A647) conjugated versions to validate the hexahistidine binding properties with spectroscopic methods. In agreement with literature values, our probes showed a lower nanomolar affinity toward a recombinant eGFP-H6 in free solution (Fig. 2 *B* and see Fig. S2 *A*) with a fast association and dissociation kinetics in the timescale of seconds (see Fig. S2 *B*).

In HEK293T, we coexpressed pairs of fluorescently tagged receptor subunits at the cell surface (Fig. 3 *A*) (11). Under certain conditions, ectopic expression of full-length IL-4Rα chains in HEK293T cells can induce an abnormal rounded shape with large amounts of receptors retained in perinuclear membrane compartments, which appeared unsuitable for microscopic FCCS analysis (see Fig. S3). Based on crystal structures of extracellular domains and our own observations (9), we reasoned that the amino acids located C-terminal of the cytoplasmic JAK1 binding site (No. 267-800, mature numbering) might only play a minor role for complex formation. Therefore, we first used a truncated IL-4Rα chain (H6-IL-4Rαm266) that exhibits improved plasma membrane localization and an extracellular accessible hexahistidine stretch (38).

To measure receptor dimerization, H6-IL-4Rαm266 was coexpressed with a second receptor subunit fused to a cytoplasmic, C-terminal eGFP (IL-2Rγ or IL-13Rα1; Fig. 3 *B*) (11). The external dye trisNTA-A647 was applied at saturating conditions (10–20 particles in the observation volume as measured by fluorescence correlation spectroscopy

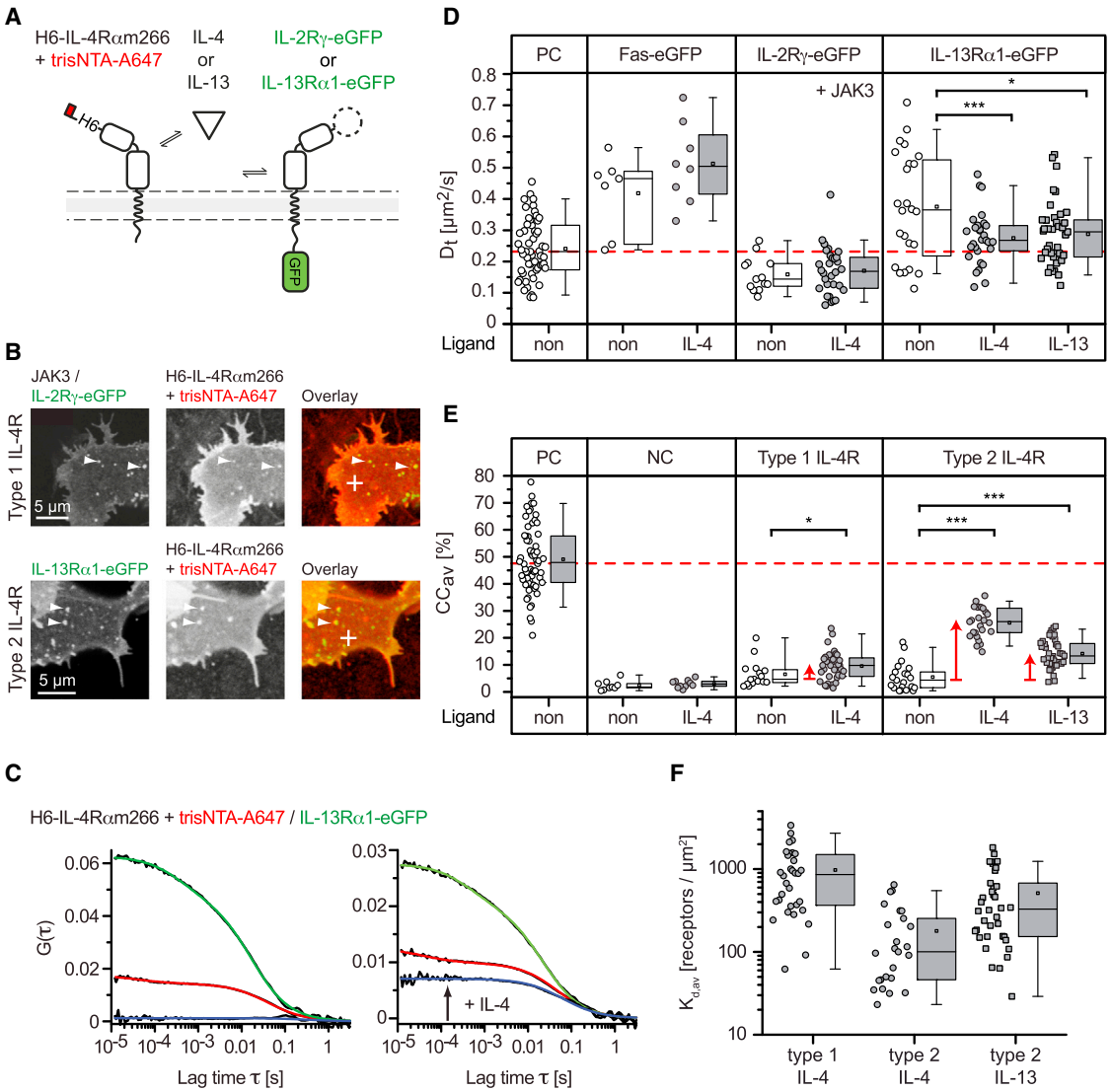

FIGURE 3 FCCS quantification of IL-4R subunit interactions in the plasma membrane. (*A*) Experimental strategy: complex formation between a truncated, trisNTA-A647-labeled H6-IL-4Rα construct and the eGFP-tagged second receptor subunit increases cross-correlation. (*B*) Confocal images (*grayscale* for single channels) showing the bottom membrane of stained HEK293T cells. Endosomes accumulating dye (*arrows*) and FCCS measurement positions (*crosses*) are indicated. (*C*) Example correlation curves showing increased cross-correlation (*blue*, *arrow*) in the presence of IL-4. (*E* and *D*) Diffusion coefficients of GFP-tagged receptors (*D*) and normalized cross-correlation amplitudes (CC_{av}) (*E*) for the doubly-tagged positive control (*PC*, H6-IL-4Rαm266-eGFP), and coexpression of H6-IL-4Rαm266 with either a negative control (NC) Fas-eGFP, IL-2Rγ-eGFP, or IL-13Rα1-eGFP. Extracellular His-tags labeled with trisNTA-A647, ligands present as indicated. Increased CC_{av} indicates complex formation. (*F*) Intramembrane dissociation constants for the three IL-4R complexes determined from the FCCS data. Box-and-whisker plots indicate second and third quartile (*box*), mean (*square*), median (*horizontal line*), and 1.5× interquartile range (*whiskers*). Asterisk (*) indicates $p < 0.05$, *** $p < 0.01$ (analysis of variance). (*Dashed red lines*) Mean of PC. To see this figure in color, go online.

corresponding to ~35–70 nM). Due to the large difference in diffusion time, the unbound dye and the much slower receptor-coupled labels could be clearly discriminated in the correlation functions (see the fast decay in the *autocorrelation curve* of the red channel, Fig. 3 *C*). The diffusion coefficient of the fast component ($D_t = 374 \pm 111$ $\mu m^2/s$; $n = 220$) corresponds well with dye molecules diffusing in bulk solution (see Table S1 in the Supporting Material). The remaining slow fraction (70–80%) was considered for cross-correlation analysis.

The mobility of the eGFP-tagged receptor chains in the plasma membrane showed some variation among the different constructs. (Fig. 3 *D*). Even in the absence of ligand, IL-2Rγ-eGFP/JAK3 complexes exhibit a reduced mobility as compared to IL-13Rα1-eGFP and the truncated construct (positive control, H6-IL-4Rαm266-eGFP), which may reflect cytoskeleton interactions (4). Applying ligand had no effect. In contrast, type-2 dimers showed a consistently reduced mobility upon ligand binding (IL-13Rα1-eGFP). The order of magnitude of this reduction is more

than one would expect for a pure dimerization and may include rearrangements of the local lipid environment of the transmembrane receptors (28). Overall, the diffusion coefficients showed significant scatter, due to the various dynamic processes simultaneously observed at the plasma membrane, e.g., endocytic trafficking.

A more robust readout for complex formation is the cross-correlation ratio (*CC*), which indicates the degree of codiffusion of the labeled H6-IL-4Rαm266 and the eGFP-tagged second receptor unit (Fig. 3 *E*). In FCCS, the actual *CC* value depends on which color channel was used for normalization. Here we show CC_{av}, the mean of CC_G and CC_R (see the Appendix), to demonstrate that the results still hold for a potentially biased abundance of receptor subunits in the two color channels. Applying IL-4 increased CC_{av} for IL-2Rγ-eGFP/JAK3 from 9.2 ± 7.0% to 13.6 ± 8.2% ($p < 0.05$), and for IL-13Rα1-eGFP from 8.3 ± 7.3% to 35.3 ± 7.9% ($p < 0.01$), whereas IL-13 produced only 17.3 ± 7.0% ($p < 0.01$) (see Table S2). The CC_{av} values showed a nearly Gaussian distribution across the measured cell populations; their first moment was positioned between zero and the maximum achievable CC_{av} level, as defined by intramolecular cross-correlation (see Fig. S4, *A* and *B*). Thus, ligand-induced complex formation was detected at the plasma membrane for all three complexes.

The magnitude of the fluorescence fluctuations in FCCS obeys a reciprocal relationship with the number of particles in the detection area; thus cellular receptor surface densities can be quantified. In our transient expressions we measured cells expressing, on average, several hundred receptors per μm^2 (see Table S2). Assuming a steady-state situation in which the law of mass action governs lateral interactions within the membrane, the abundance of each binding partner from autocorrelation and the fraction of double-labeled dimers derived from cross-correlation enabled us to calculate two-dimensional dissociation constants (see Appendix). Because the binding partners are confined within the two-dimensional membrane plane, these K_d values are expressed in dimensions of receptors per area. Because the external cytokine ligand was applied in excess, these values directly reflect the receptor surface density for which recruitment occurs with a probability of 50%.

We obtained $K_{d,2D} = 180 \pm 40$ receptors/μm^2 for the IL-4Rα:IL-4/IL-13Rα1 interaction, 480 ± 100 receptors/μm^2 for IL-4Rα/IL-13:IL-13Rα1, and 1000 ± 170 receptors/μm^2 for IL-4Rα:IL-4/IL-2Rγ (Fig. 3 *F* and see Table S2). Calibration of the cross-correlation with autocorrelation amplitudes of either the eGFP or the A647 channel produced consistent results (see Fig. S4 *C*). Notably, the potency of the two different ligands IL-4 and IL-13 to induce a type-2 complex reflects their relative signaling strength (see Fig. S1). However, considering physiological surface expression levels of several receptor molecules per μm^2 (39), the order of magnitude of these K_d values for all three receptor types is remarkably high, rendering dimerization at the plasma membrane very ineffective and short-lived.

Encouraged by these results, we finally aimed to confirm ligand-induced subunit recruitment for the full-length IL-4Rα chain. Because the type-1 interaction was already weak, we revisited the type-2 configuration. As is the case for the full-length GFP-tagged IL-4Rα constructs themselves, coexpression IL-13Rα1-eGFP with either nontagged or His-tagged IL-4Rα led to the very same rounded shape and massive retention in a perinuclear membrane compartment, presumably the endoplasmic reticulum (see Fig. S3 and Fig. S5 *A*). However, a small fraction of cells showed a stretched appearance with sufficient colocalization at the cell surface for FCCS (see Fig. S5 *B*). A difference in diffusion between the truncated positive control H6-IL-4Rαm266-eGFP ($D_t = 0.24 \pm 0.1$ μm^2/s; $n = 121 \times 15$ s) and the full-length H6-IL-4Rα ($D_t = 0.2 \pm 0.06$ μm^2/s; $n = 67 \times 15$ s) was small and unchanged when occupied by cytokine ligands. The FCCS measurements suffered from a lower surface density of full-length H6-IL-4Rα for which we hardly reached 100 receptors per μm^2 and, thus, stayed systematically at $< K_d$. Nevertheless, in agreement with previous results, for both ligands we measured a significant, ligand-induced increase in cross-correlation (see Fig. S5 *C*). The magnitude of this shift was comparable with the experiments using the truncated receptors. The intracellular domains thus play, at most, a minor role for ligand-induced IL-4R dimerization.

IL-4R subunits accumulate in early sorting and recycling endosomes stably anchored below the plasma membrane

To avoid confounding effects of endogenous proteins, we first studied the subcellular distribution of ectopically expressed type-1 receptor subunits. Confocal live cell imaging of nonstimulated cells showed that JAK3-eGFP is recruited to the plasma membrane by IL-2Rγ (Fig. 4 *A*, *top panels*) and is in turn required for efficient IL-2Rγ membrane localization (31) (Fig. 4 *A*, *bottom panels*).

In cells where the IL-2Rγ receptors were fully saturated, increasing levels of nonbound JAK-eGFP produced a homogeneous background in the cytoplasm. In contrast, the IL-2Rγ/JAK3 complexes at the plasma membrane were not homogeneously distributed but concentrated into punctate, specklelike structures across a wide range of expression levels (Fig. 4 *A*, *right panels*). The distribution of IL-2Rγ/JAK3-containing speckles was independent of stimulation and their size and positions were remarkably stable at the timescale of minutes (Fig. 4 *B*, and see Movie S1 and Fig. S6). Because TIRF illumination is confined to ~100 nm proximal to the glass support, these stable structures must be located in the cell cortex very close to the plasma membrane.

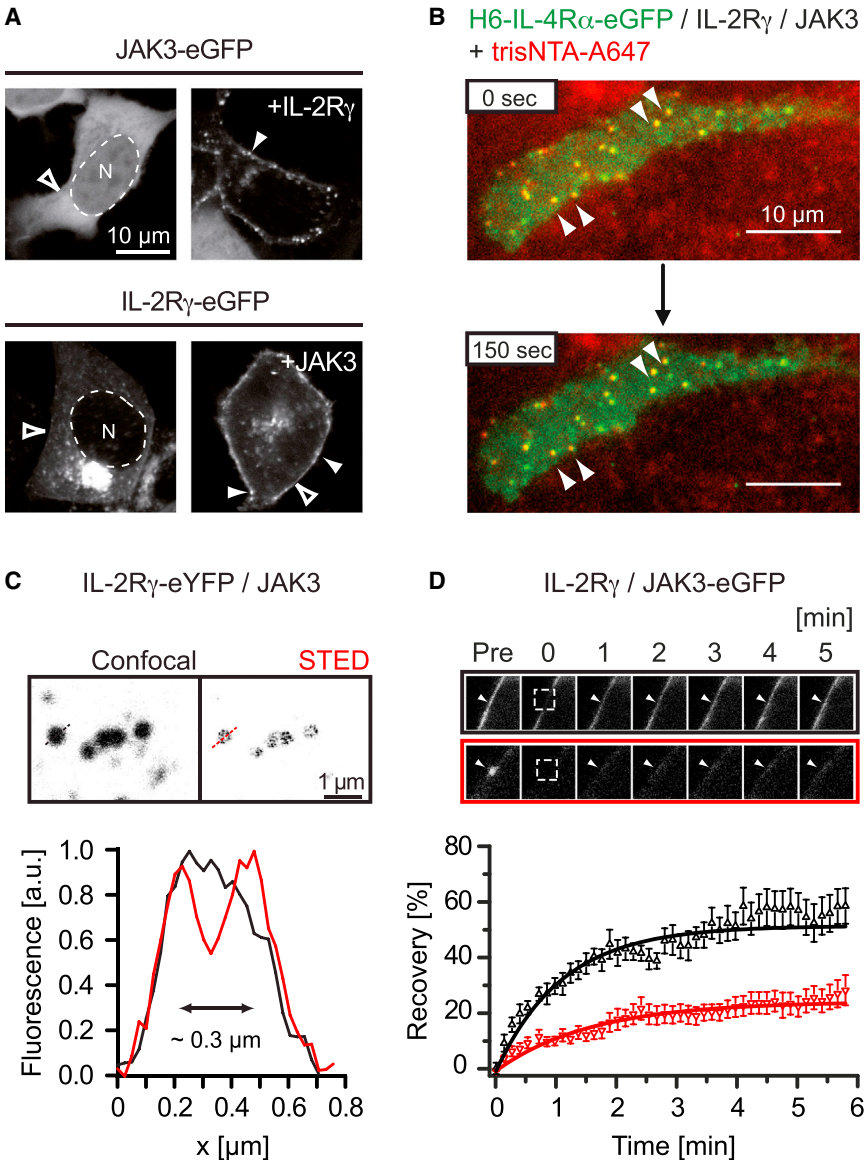

FIGURE 4 IL-4R subunits accumulate in submembrane vesicles. (*A*) eGFP-tagged IL-2Rγ requires JAK3 for partitioning to the plasma membrane (*upper panels*) and JAK3-GFP is recruited to the membrane by IL-2Rγ (*lower panels*). In both cases, eGFP fluorescence concentrates in membrane-associated speckles (*grayscale* for GFP fluorescence). (*B*) Cells transiently expressing type-1 IL-4R subunits were stained with 90 nM trisNTA-A647. Time-lapse imaging at 37°C under TIR illumination shows that surface-expressed IL-4Rα chains accumulate vesicles located within a few hundred nanometers of the undersurface of the cells. Their position remains stable over several minutes (see also Movie S1 in the Supporting Material). Arrowhead positions were kept fixed relative to the frames. (*C*) STED imaging of speckles. Representative confocal (*black*) and STED (*red*) intensity profiles reveal their vesicular nature. (*D*) FRAP of IL-2Rγ/JAK3-eGFP complexes. Prebleach images and recovery shown for two representative examples. Vesicles do not recover during the observation time. The immobile fraction is increased in ROIs containing vesicles (*red*) relative to the uniform plasma membrane (*black*). $n = 10$ cells each, error bars indicate mean ± SE. To see this figure in color, go online.

In standard confocal images, the speckles exhibited a pointlike aspect. However, subdiffraction imaging at ~90-nm resolution using STED microscopy revealed vesicular structures with a diameter of ~300 nm (Fig. 4 *C*). To characterize the dynamic behavior of IL-2Rγ/JAK3-eGFP complexes within these structures, we used FRAP (Fig. 4 *D*). The observed recovery time constants of 45 s (plain membrane) and 66 s (ROI containing a vesicle) are consistent with lateral, intramembrane diffusion of IL-2Rγ/JAK3-eGFP in the plasma membrane, but not with recovery modes relying on fast dynamic exchange between the receptor-bound and cytoplasmic pools of JAK3, thus resembling the dynamics of JAK1 (35). However, the immobile fraction was increased from 45 to 78% within ROIs containing both membrane and vesicle, reflecting the complete failure of fluorescence recovery in the vesicles during the observation time (Fig. 4 *D*). Thus, IL-2Rγ/JAK3-eGFP complexes accumulate in vesicular compartments anchored just underneath the plasma membrane, which are not in diffusive exchange with the plasma membrane pool.

We next determined the signature of endosomal cofactors (Fig. 5 *A* and see Fig. S7 *A*). To avoid signals from perinuclear compartments associated with trafficking of nascent receptor chains, we used JAK3-eGFP as a bonafide marker to unambiguously identify the subset of IL-2Rγ-containing, plasma-membrane-associated endosomes. Congruent patterns of positive signals were observed with the early endosomal markers mRFP-Rab5 (96 ± 2% of speckles showing costaining) and EEA1 (84 ± 8%) as well as mCherry-Rab11 (91 ± 2%), a marker of the recycling compartment. Based on these fractions, at least 80% of all JAK3 positive endosomes must contain both Rab5 and Rab11. In contrast,

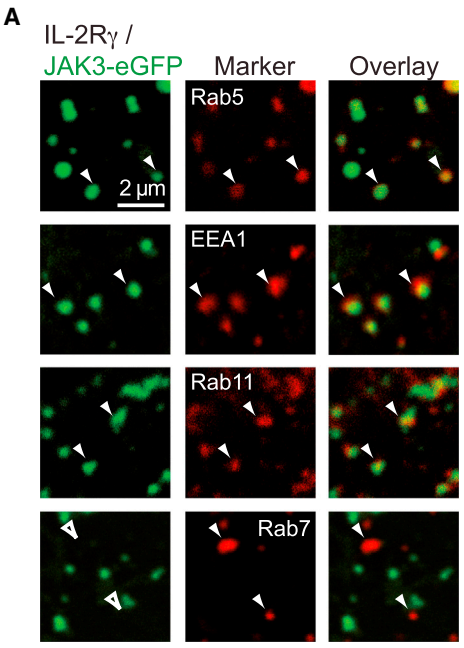

FIGURE 5 Cortical endosomes decorated with markers for early sorting and recycling. (*A*) IL-2Rγ/JAK3 complexes colocalize with markers (*red*) for early sorting (EEA1, mRFP-Rab5) and recycling (mCherry-Rab11) endosomes, but not for the degradation pathway (mRFP-Rab7). (*B*) Quantification of marker colocalization including markers for late endosomal or lysosomal compartments (Lamp1, Lysotracker LT). Error bars indicate SD. To see this figure in color, go online.

colocalization with the late endosomal and lysosomal markers mRFP-Rab7, Lamp1, or Lysotracker was <20% (Fig. 5 *B* and see Table S3).

Similarly, when coexpressed, IL-13Rα1 and IL-2Rγ were trafficked into the same compartments, suggesting that type-1 and type-2 components follow the same endocytosis pathway (see Fig. S7 *B*). Thus, in HEK293T cells all three IL-4R subunits reside in a subpopulation of regular early sorting and recycling endosomes stably anchored in the cell cortex, which we accordingly termed cortical endosomes (CEs).

IL-4R subunit internalization and JAK/STAT signal transduction

Coexpression studies showed that, under steady-state conditions, IL-4R subunits accumulate in CEs already in the absence of ligand. To test whether the ligand-occupied receptor follows the same endocytosis route, we used our previously described fluorescently labeled IL-4-A647 probe (11). HEK293T cells overexpressing type-1 IL-4R subunits were loaded with ligand at 4°C, washed, and then fluorescence redistribution followed at room temperature. As long as membrane dynamics remained blocked, the distribution of IL-4-A647 bound to full-length IL-4Rα at the cell surface appeared homogenous (Fig. 6 *A*, *top row*). However, IL-4-A647 accumulated rapidly in the CEs within several minutes of temperature release (Fig. 6 *A*, *bottom rows*). A similar redistribution kinetics was observed when expressing the truncated receptor IL-4Rαm266 (see Fig. S8 *A*), consistent with observations in BaF3 cells showing that internalization of ligand does not require signaling active receptors (40).

Using trisNTA-A647 as a ligand independent tracer (Fig. 2) enabled us to study the effect of receptor occupancy on the trafficking kinetics (see Fig. S8, *B* and *C*). The N-terminus is located distant from the IL-4/IL-13 binding site; trisNTA labeling and cytokine binding are therefore orthogonal (23,24). We tracked internalization of receptors preloaded with trisNTA-A647 by photon counting after temperature release (Fig. 6 *B*). The saturation value for dye loaded via H_6-IL-4Rα was only 30% of that loaded by H_6-IL-2Rγ. A nonspecific background (9.5 ± 4%) was determined by comparing H_6-IL-2Rγ with nontagged IL-2Rγ at time-point 30 min. The uptake kinetics could be fitted by saturating exponentials with time constants of 6.6 ± 0.7 min for H_6-IL-2Rγ and 8.5 ± 1.3 min for H_6-IL-4Rα, which is qualitatively comparable to the internalization of labeled IL-4 ligand by untagged receptor (Fig. 6 *A*). Importantly, H_6-IL-4Rα internalization was independent of IL-4 occupancy (Fig. 6 *C*).

To compare trafficking with IL-4R-mediated JAK/STAT pathway activation, we performed a corresponding pulse-chase experiment: HEK293T cells transiently expressing STAT6 were saturated with IL-4 on ice, washed, and lysed after increasing time-points of temperature release (37°C). The lysates were analyzed by sodium dodecyl sulfate-polyacrylamide gel electrophoresis and probed for STAT6 phosphorylation (Fig. 6 *D*). The response curve followed a sigmoid shape that could be fitted to a logistic function (t_0 = 12.6 min). Note that the onset of the response is slightly delayed with respect to receptor trafficking. The response persisted for >30 min without reaching a plateau.

Finally, we assayed for activated JAK/STAT pathway components. Because antibodies for the STAT6 binding site of activated IL-4Rα were not available, we probed for the adjacent phospho-tyrosine Y497, a docking site for the

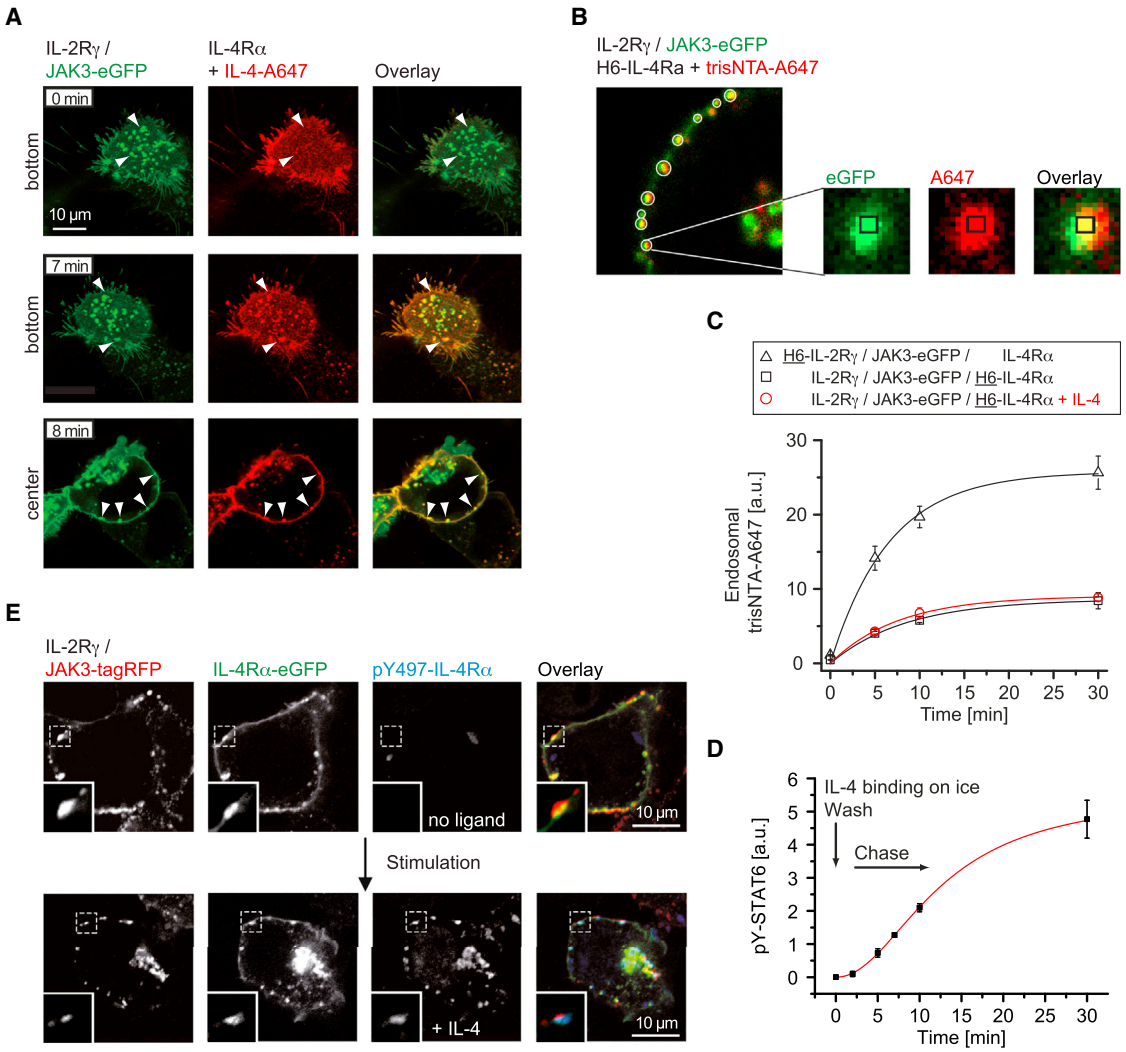

FIGURE 6 Constitutive internalization concentrates ligands and receptors within cortical signaling endosomes. (*A*) Ligand endocytosis imaged in live cells. Staining with IL-4-A647 at 4°C is first homogeneous (0 min), but accumulates within CEs upon temperature release (7 and 8 min, *arrowheads*). (*B*) Trafficking of receptor subunits monitored by the His-tag-specific trisNTA-A647. (*C*) Kinetics of type-1 IL-4R subunits (*triangles*, H6-IL-2Rγ; *squares*, H6-IL-4Rα). H6-IL-4Rα uptake also measured in the presence of IL-4 (*circles*). Dye accumulation in endosomes plotted versus incubation time. Error bars indicate mean ± SE. (*D*) STAT6 phosphorylation kinetics after pulsed stimulation with IL-4. Error bars indicate SD. (*E*) Immunostainings showing the presence of both type-1 IL-4R subunits and activated IL-4Rα (pY497) within plasma-membrane-associated cortical endosomes.

insulin receptor substrate 1/2 (16) whose activation closely parallels JAK/STAT pathway activation (11). IL-4Rα colocalized with JAK3-positive vesicles already in the absence of ligand. However, pY497 staining was IL-4-dependent and preferentially colocalized at the vesicles with both receptor subunits (Fig. 6 *E*). Recalling the concept of signaling endosomes established for several other pathways (41,42), these observations suggested that CEs might play a similar role for JAK/STAT signal transduction.

DISCUSSION

Using IL-4R as an example, we report, to our knowledge for the first time, lateral affinities of receptor subunit recruitment for members of the hematopoietic superfamily of cytokine receptors in the plasma membrane. Although ligand-induced dimerization was detected for the full-length IL-4Ra chain, a quantitative K_d determination requires the use of a truncated IL-4Rα construct that shows the same trafficking behavior as the full-length receptor but exhibits improved plasma membrane partitioning. The construct lacks the STAT6 docking sites required for downstream signaling; our reporter gene assay therefore shows that it is fully competitive toward the endogenous type-2 signaling machinery. Because these experiments were performed under excess of stimulating cytokine ligand, the truncated IL-4Rα construct must compete at the level of dimerization and not for capturing ligands from bulk solution. However, the cytoplasmic tail of the truncated IL-4Rα still contains a functional box-1 motif required for JAK1 binding. While

JAK3 was supplemented to saturate IL-2Rγ, receptor dimerization was measured in the presence of endogenous levels of JAK1 and Tyk2, for which the exact receptor occupancy (at IL-4Rα and IL13Rα1, respectively) could not be determined. Further studies will be required to address systematically whether JAKs contribute to the stability of the activated IL-4R complex.

Under this premise, we find that the ranking of $K_{d,2D}$ values reflects the relative signal potencies of the otherwise identical type-2 receptor complexes induced by IL-4 or IL-13, supporting a direct link between complex stability and signal strength. However, this ranking does not correlate with the affinities of isolated ectodomains in free solution, where the preformed IL-4/IL-4Rα complex recruits IL-2Rγ and IL-13Rα1 ectodomains with a comparably low affinity (0.5–4 μM) (24,25), whereas a preformed IL-13/IL-13Rα1 complex recruits the IL-4Rα ectodomain with higher affinity (20 nM) (24). It therefore remains unclear how to account for the entropic contributions when translating interactions between soluble forms into the two-dimensional membrane context.

The lateral, intramembrane $K_{d,2D}$ values measured by FCCS were of the order of several hundred receptors per μm^2 and could be only measured in cells expressing correspondingly high surface densities (see Table S2). In our HEK293T model, we verified that IL-2Rγ mRNA is downregulated (Fig. 1 *A*) and that endogenous IL-4Rα protein is below the detection limit (see Fig. S3 *A*). Therefore, a potential background of nontagged receptors, and hence an artificially reduced K_d, could only affect the type-2 configuration for which we nevertheless obtained the highest cross-correlation. Thus, our observation that the affinity of the type-1 complexes is extremely low, is conservative. The fact that the IL-4R type-1 interaction is weak was previously proposed (12). However, with hindsight, these experiments did not distinguish between receptor pools at the cell surface and those within CEs. The absolute K_d values are two orders of magnitude above typical cytokine receptor expression levels (500–5000 molecules per cell with ~1000 μm^2 surface correspond to a density of 0.5–5 receptors per μm^2) (12,39). This discrepancy is striking considering that, even under full ligand occupancy, such affinities would produce only a negligible number of ternary, signaling active IL-4R dimers in the plasma membrane.

The weak affinity for receptor subunit dimerization implies that a transient or locally confined cellular concentration mechanism is required to efficiently drive IL-4R dimerization and establish a robust JAK/STAT response. Here we propose that constitutive internalization might be such a mechanism. Confocal, STED, and TIRF imaging showed that the receptor subunits accumulate in small vesicles stably positioned close to plasma membrane. Marker expression defined these vesicles as a subpopulation of regular early sorting and recycling endosomes that we termed CEs. We then quantified the precise uptake kinetics into CEs for each of the type-1 receptor subunits with rate constants of 6–9 min. As expected from their CE localization in nonstimulated cells, internalization does not require pathway activation because the rate constants of IL-4Rα were unchanged upon ligand binding.

In comparison, the JAK/STAT pathway response is rather slow: the onset of STAT6 phosphorylation is delayed by 1–2 min; the time to reach half-maximum of activation (12.5 min) is of the same order of magnitude as the rate constants for internalization. Even more a surprise, the signal steadily increased far beyond the expected residence time of the complex. IL-4 bound to IL-4Rα has a half-life of ~5.5 min (18). Neglecting the small enthalpic contributions of the second receptor chain when forming dimers (24,25), during the course of the pulse chase experiment (30 min) most of the ligand should be dissociated if the complexes remained at the cell surface. Thus, to maintain such a long-lasting output in response to a transient stimulus, activated receptor complexes must either remain stable or continuously reform within confined subcellular compartments, e.g., in the CEs. Such a scenario is further supported by the preferential localization of activated IL-4Rα chain within CEs.

Recently, it was observed in T-cells that JAK/STAT pathway activation by IL-2Rγ-sharing IL-7R involves partitioning into cholesterol-enriched microdomains, transient cytoskeleton interactions, and the formation of signalosomes in the plasma membrane (28,43). Although such signalosomes could constitute a potential concentration mechanism for CKR at the plasma membrane, we see no such aggregations in our epithelial HEK293T model. Intriguingly, in the IL-2 context, lipid raft partitioning of IL-2Rγ has also been linked to receptor endocytosis (44). IL-2Rγ is internalized by a specific clathrin- and caveolin-independent endocytosis pathway (45,46) that involves local actin polymerization (27). The actin-mediated mode of endocytosis may readily explain the stable localization of CEs within the cell cortex, which may involve a densely packed actin mesh.

Although these cell biological mechanisms have yet to be experimentally verified, our observations raise the possibility that CEs provide a subcellular concentration function for the formation of activated receptor dimers and thus constitute signaling platforms not yet described for this receptor class (41). This mode of activation would intrinsically buffer the JAK/STAT pathway against fluctuating ligand concentrations and lateral heterogeneities associated with a dynamic, microdomain patterning of the plasma membrane.

APPENDIX: K_D DETERMINATION FROM FCCS DATA

We estimated the two-dimensional dissociation constant for lateral recruitment of receptor subunits under saturating ligand concentrations. Fitting

and background correction returns the fluctuation amplitudes $G_G(0)$, $G_R(0)$, and $G_x(0)$, each of which reflect the inverse average number of observed particles N in the respective detection volume, V_{eff} (47). The two-component fit resolves the fraction f of molecules contributing to fast diffusion in bulk solution (three-dimensional, e.g., unbound ligand trisNTA-A647) and the fraction $(1-f)$ contributing to the slow diffusion within the membrane plane (two-dimensional, e.g., trisNTA-A647 labeled receptor). The average number of receptors diffusing in the membrane plane is

$$\begin{aligned} N_G &= (1-f_G)G_G^{-1}(0), \\ N_R &= (1-f_R)G_R^{-1}(0). \end{aligned} \tag{A1}$$

Note that capital letters (G, R) index the color channels (fitting derived parameters) whereas small letters (g, r) index the type of label (true molecular parameters). We treated the eGFP channel accordingly due to a stable fast fraction with a correlation time in the millisecond range, which was absent in the cross-correlation functions, and therefore unrelated to receptor diffusion. We verified with a positive control (PC, trisNTA-A647 labeled NHis-IL4Rm266-eGFP) that this treatment yields the exact same receptor density when measuring the double-labeled receptors simultaneously in both color channels ($N_R V_{\text{eff},G}/N_G V_{\text{eff},R} = 0.99 \pm 0.04$; mean $\pm$ SE; $n = 57$). The focal volume in the eGFP channel $V_{\text{eff},G}$ was determined with a diffusion standard (AlexaFluor 488; Life Technologies (= A488) in 10 mM Tris, pH 8, $D = 435\ \mu\text{m}^2/\text{s}$ (48)), which delivers a measure for the beam waist

$$\omega_{0,G} = \sqrt{4D \cdot \tau_{\text{diff}}}. \tag{A2}$$

The chromatic mismatch between the eGFP and the A647 channel was derived from the ratio of the slow, membrane-related diffusion times measured for the double labeled PC ($\tau_{\text{diff},R}/\tau_{\text{diff},G} = 1.30 \pm 0.076$; mean $\pm$ SE; $n = 57$). The autocorrelation amplitudes can be calibrated into two-dimensional receptor densities for both color channels:

$$\begin{aligned} C_g &= \frac{N_G}{\pi \cdot \omega_{0,G}^2}, \\ C_r &= \frac{N_R}{\pi \cdot \omega_{0,R}^2} = \frac{N_R}{1.30 \cdot \pi \cdot \omega_{0,G}^2}. \end{aligned} \tag{A3}$$

We defined CC as the ratio of simultaneously recorded cross- and autocorrelation amplitudes (11,47,49),

$$\begin{aligned} CC_G &= G_x(0) \cdot N_G, \\ CC_R &= G_x(0) \cdot N_R. \end{aligned} \tag{A4}$$

To derive binding relevant data, CC values must be rescaled to the accessible CC range defined by intramolecular cross-correlation positive control (PC) and a noninteracting negative control (NC) measured under the same instrumental conditions:

$$CC_{G,n} = \frac{CC_G - CC_{NC}}{CC_{PC} - CC_{NC}}. \tag{A5}$$

Although we show that ligands are unable to recruit a noninteracting NC (Fas receptor chain), the corresponding cellular CC_{NC} values introduced scatter. We therefore checked numerically that the crosstalk-related contribution to the cross-correlation amplitude (5% of the eGFP fluorescence appears in the A647 channel) was negligible by using a recently developed mathematical formalism (47,50). With $CC_{NC} = 0$, the measured and normalized CC_n values directly represent the fraction ligand bound,

$$\begin{aligned} CC_{G,n} &= \frac{CC_G}{CC_{PC}} = \frac{N_{gr}}{N_r}, \\ CC_{R,n} &= \frac{CC_R}{CC_{PC}} = \frac{N_{gr}}{N_g}, \end{aligned} \tag{A6}$$

with respect to the total number of particles labeled in the orthogonal color (not used for normalization: $G \rightarrow r$ and $R \rightarrow g$).

The dissociation constant is given by the law of mass action containing the equilibrium (or steady-state) concentrations of free and bound receptors, which can be expressed by particle numbers contained in a uniform observation volume V_{eff},

$$K_d = \frac{1}{V_{\text{eff}}} \frac{N_{g,\text{free}} \cdot N_{r,\text{free}}}{N_{gr}} = \frac{1}{V_{\text{eff}}} \frac{\left(N_g - N_{gr}\right)\left(N_r - N_{gr}\right)}{N_{gr}}. \tag{A7}$$

The number of complexes can be derived from the normalized cross-correlation ratio CC_n. To avoid mixing up differently sized observation volumes, one has to be consistent with the color channel. For example, using $CC_{R,n}$ gives

$$K_{d,R} = \frac{1}{V_{\text{eff},R}} \frac{\left(N_g - N_g CC_{R,n}\right)\left(N_r - N_g CC_{R,n}\right)}{N_g CC_{R,n}}. \tag{A8}$$

and rearranged gives

$$K_{d,R} = \frac{1}{V_{\text{eff},R}} \left(\frac{1}{CC_{R,n}} - 1\right)\left(N_r - N_g CC_{R,n}\right). \tag{A9}$$

The true particle numbers N_r as well as N_g now both refer to $V_{\text{eff},R}$ and can be directly derived from fluorescence correlation spectroscopy amplitudes. However, due to chromatic mismatch, one must account for the differently sized observation volumes

$$K_{d,R} = \frac{1}{V_{\text{eff},R}} \left(\frac{1}{CC_{R,n}} - 1\right)\left(N_R - \frac{V_{\text{eff},R}}{V_{\text{eff},G}} N_G CC_{R,n}\right), \tag{A10}$$

which is, finally,

$$\begin{aligned} K_{d,R} &= \left(\frac{1}{CC_{R,n}} - 1\right)\left(C_r - C_g \cdot CC_{R,n}\right), \\ K_{d,G} &= \left(\frac{1}{CC_{G,n}} - 1\right)\left(C_r - C_g \cdot CC_{G,n}\right). \end{aligned} \tag{A11}$$

Because the problem is symmetrical, the corresponding expression referring to $V_{\text{eff},G}$ can be easily derived by swapping the indices. Here C_g and C_r represent the true calibrated concentrations (receptor densities) as derived from the autocorrelation measurements.

The distinction between $K_{d,G}$ and $K_{d,R}$ is of a purely technical nature. In practice, when chromatic mismatch and uneven expression levels do not accidentally compensate each other, $CC_{G,n}$ and $CC_{R,n}$ values from the same binding reaction are expected to be different. Using the channel with larger cross-correlation ($CC_{n,\max}$) is expected to be more reliable in terms of stochastic errors. Nevertheless, both ways of determining the K_d should be consistent. As shown in Fig. S4 *C*, the experimental values for $K_{d,G}$ and $K_{d,R}$ show a large degree of correlation (slope ~1). However, the K_d estimation becomes increasingly uncertain when the measured CC value approaches the minimum (here ~0%) or maximum (here ~50%) of the experimentally determined, accessible CC range. The reported final K_d

values comprise the arithmetic mean between average $K_{d,G}$ and $K_{d,R}$ measured for a population of 20–30 cells.

SUPPORTING MATERIAL

Eight figures, three tables, and one movie are available at http://www.biophysj.org/biophysj/supplemental/S0006-3495(14)01107-2.

We thank John J. O'Shea for providing JAK3 constructs, Marino Zerial for providing Rab constructs, Bernard Hoflack for antibodies, and Attila Szanto and Lazlo Nagy for the STAT6-inducible reporter genes. We thank C. Herold for providing a MATLAB script, and K. Crell, S. Herrmann, S. Knappe, S. v. Kannen, R. Perez Palencia, and Bea Scheffer for their committed technical assistance.

R.W. is grateful for receiving a postdoctoral fellowship from the Alexander von Humboldt Foundation (Germany). The use of a Confocor3 was supported by Carl Zeiss AG (Jena, Germany). This work was supported by a Center for Regenerative Therapies Dresden seed grant (to K.K., C.B., P.S., and T.W.) and Deutsche Forschungsgemeinschaft priority program No. TRR67 (to H.G., T.W., and P.S.).

REFERENCES

1. Boulay, J. L., J. J. O'Shea, and W. E. Paul. 2003. Molecular phylogeny within type I cytokines and their cognate receptors. *Immunity.* 19:159–163.
2. Haan, C., C. Rolvering, …, H. G. Zerwes. 2011. Jak1 has a dominant role over Jak3 in signal transduction through γc-containing cytokine receptors. *Chem. Biol.* 18:314–323.
3. Leonard, W. J., and J. J. O'Shea. 1998. Jaks and STATs: biological implications. *Annu. Rev. Immunol.* 16:293–322.
4. Pillet, A. H., V. Lavergne, …, T. Rose. 2010. IL-2 induces conformational changes in its preassembled receptor core, which then migrates in lipid raft and binds to the cytoskeleton meshwork. *J. Mol. Biol.* 403:671–692.
5. Brown, R. J., J. J. Adams, …, M. J. Waters. 2005. Model for growth hormone receptor activation based on subunit rotation within a receptor dimer. *Nat. Struct. Mol. Biol.* 12:814–821.
6. Remy, I., I. A. Wilson, and S. W. Michnick. 1999. Erythropoietin receptor activation by a ligand-induced conformation change. *Science.* 283:990–993.
7. Weidemann, T., S. Hoefinger, and M. Auer. 2009. Signaling of IL-4R, a typical class I cytokine receptor: what defines the quiescent state? *In* Handbook of Cell Signaling. E. Dennis and R. Bradshaw, editors. Elsevier Press, New York.
8. Whitty, A., and T. V. Riera. 2008. New ways to target old receptors. *Curr. Opin. Chem. Biol.* 12:427–433.
9. Worch, R., C. Bökel, …, T. Weidemann. 2010. Focus on composition and interaction potential of single-pass transmembrane domains. *Proteomics.* 10:4196–4208.
10. Wang, X., P. Lupardus, …, K. C. Garcia. 2009. Structural biology of shared cytokine receptors. *Annu. Rev. Immunol.* 27:29–60.
11. Weidemann, T., R. Worch, …, P. Schwille. 2011. Single cell analysis of ligand binding and complex formation of interleukin-4 receptor subunits. *Biophys. J.* 101:2360–2369.
12. Whitty, A., N. Raskin, …, L. C. Burkly. 1998. Interaction affinity between cytokine receptor components on the cell surface. *Proc. Natl. Acad. Sci. USA.* 95:13165–13170.
13. Giese, B., C. Roderburg, …, G. Müller-Newen. 2005. Dimerization of the cytokine receptors gp130 and LIFR analyzed in single cells. *J. Cell Sci.* 118:5129–5140.
14. Neugart, F., A. Zappe, …, L. Graeve. 2009. Detection of ligand-induced CNTF receptor dimers in living cells by fluorescence cross correlation spectroscopy. *Biochim. Biophys. Acta.* 1788:1890–1900.
15. Kelly-Welch, A. E., E. M. Hanson, …, A. D. Keegan. 2003. Interleukin-4 and interleukin-13 signaling connections maps. *Science.* 300:1527–1528.
16. Nelms, K., A. D. Keegan, …, W. E. Paul. 1999. The IL-4 receptor: signaling mechanisms and biologic functions. *Annu. Rev. Immunol.* 17:701–738.
17. Mueller, T. D., J. L. Zhang, …, A. Duschl. 2002. Structure, binding, and antagonists in the IL-4/IL-13 receptor system. *Biochim. Biophys. Acta.* 1592:237–250.
18. Wang, Y., B. J. Shen, and W. Sebald. 1997. A mixed-charge pair in human interleukin 4 dominates high-affinity interaction with the receptor α-chain. *Proc. Natl. Acad. Sci. USA.* 94:1657–1662.
19. Zhang, J. L., I. Simeonowa, …, W. Sebald. 2002. The high-affinity interaction of human IL-4 and the receptor α-chain is constituted by two independent binding clusters. *J. Mol. Biol.* 315:399–407.
20. Duppatla, V., M. Gjorgjevikj, …, W. Sebald. 2013. IL-4 analogues with site-specific chemical modification at position 121 inhibit IL-4 and IL-13 biological activities. *Bioconjug. Chem.* 25:52–62.
21. Grunewald, S. M., A. Werthmann, …, A. Duschl. 1998. An antagonistic IL-4 mutant prevents type I allergy in the mouse: inhibition of the IL-4/IL-13 receptor system completely abrogates humoral immune response to allergen and development of allergic symptoms in vivo. *J. Immunol.* 160:4004–4009.
22. Laporte, S. L., C. M. Forsyth, …, R. M. Stroud. 2005. De novo design of an IL-4 antagonist and its structure at 1.9 Å. *Proc. Natl. Acad. Sci. USA.* 102:1889–1894.
23. Hage, T., W. Sebald, and P. Reinemer. 1999. Crystal structure of the interleukin-4/receptor α-chain complex reveals a mosaic binding interface. *Cell.* 97:271–281.
24. LaPorte, S. L., Z. S. Juo, …, K. C. Garcia. 2008. Molecular and structural basis of cytokine receptor pleiotropy in the interleukin-4/13 system. *Cell.* 132:259–272.
25. Zhang, J. L., M. Buehner, and W. Sebald. 2002. Functional epitope of common γ-chain for interleukin-4 binding. *Eur. J. Biochem.* 269:1490–1499.
26. Grassart, A., A. Dujeancourt, …, N. Sauvonnet. 2008. Clathrin-independent endocytosis used by the IL-2 receptor is regulated by Rac1, Pak1 and Pak2. *EMBO Rep.* 9:356–362.
27. Sauvonnet, N., A. Dujeancourt, and A. Dautry-Varsat. 2005. Cortactin and dynamin are required for the clathrin-independent endocytosis of γ_c cytokine receptor. *J. Cell Biol.* 168:155–163.
28. Tamarit, B., F. Bugault, …, T. Rose. 2013. Membrane microdomains and cytoskeleton organization shape and regulate the IL7-receptor signalosome in human CD4 T-cells. *J. Biol. Chem.* 288:8691–8701.
29. Rink, J., E. Ghigo, …, M. Zerial. 2005. Rab conversion as a mechanism of progression from early to late endosomes. *Cell.* 122:735–749.
30. Vonderheit, A., and A. Helenius. 2005. Rab7 associates with early endosomes to mediate sorting and transport of Semliki forest virus to late endosomes. *PLoS Biol.* 3:e233.
31. Hofmann, S. R., A. Q. Lam, …, J. J. O'Shea. 2004. Jak3-independent trafficking of the common γ-chain receptor subunit: chaperone function of Jaks revisited. *Mol. Cell. Biol.* 24:5039–5049.
32. Lata, S., M. Gavutis, …, J. Piehler. 2006. Specific and stable fluorescence labeling of histidine-tagged proteins for dissecting multi-protein complex formation. *J. Am. Chem. Soc.* 128:2365–2372.
33. Lata, S., A. Reichel, …, J. Piehler. 2005. High-affinity adaptors for switchable recognition of histidine-tagged proteins. *J. Am. Chem. Soc.* 127:10205–10215.
34. Michel, M., I. Raabe, …, C. Bökel. 2011. Local BMP receptor activation at adherens junctions in the *Drosophila* germline stem cell niche. *Nat. Commun.* 2:415.
35. Giese, B., C. K. Au-Yeung, …, G. Müller-Newen. 2003. Long term association of the cytokine receptor gp130 and the Janus kinase Jak1 revealed by FRAP analysis. *J. Biol. Chem.* 278:39205–39213.

36. Sprague, B. L., R. L. Pego, …, J. G. McNally. 2004. Analysis of binding reactions by fluorescence recovery after photobleaching. *Biophys. J.* 86:3473–3495.

37. Müller, P., P. Schwille, and T. Weidemann. 2014. PyCorrFit—generic data evaluation for fluorescence correlation spectroscopy. *Bioinformatics.* 30:2532–2533.

38. Hintersteiner, M., T. Weidemann, …, M. Auer. 2008. Covalent fluorescence labeling of His-tagged proteins on the surface of living cells. *ChemBioChem.* 9:1391–1395.

39. Park, L. S., D. Friend, …, D. L. Urdal. 1987. Characterization of the human B cell stimulatory factor 1 receptor. *J. Exp. Med.* 166:476–488.

40. Friedrich, K., W. Kammer, …, W. Sebald. 1999. The two subunits of the interleukin-4 receptor mediate independent and distinct patterns of ligand endocytosis. *Eur. J. Biochem.* 265:457–465.

41. Platta, H. W., and H. Stenmark. 2011. Endocytosis and signaling. *Curr. Opin. Cell Biol.* 23:393–403.

42. Sadowski, L., I. Pilecka, and M. Miaczynska. 2009. Signaling from endosomes: location makes a difference. *Exp. Cell Res.* 315:1601–1609.

43. Rose, T., A. H. Pillet, …, J. Thèze. 2010. Interleukin-7 compartmentalizes its receptor signaling complex to initiate CD4 T lymphocyte response. *J. Biol. Chem.* 285:14898–14908.

44. Lamaze, C., A. Dujeancourt, …, A. Dautry-Varsat. 2001. Interleukin 2 receptors and detergent-resistant membrane domains define a clathrin-independent endocytic pathway. *Mol. Cell.* 7:661–671.

45. Mayor, S., and R. E. Pagano. 2007. Pathways of clathrin-independent endocytosis. *Nat. Rev. Mol. Cell Biol.* 8:603–612.

46. Subtil, A., A. Hémar, and A. Dautry-Varsat. 1994. Rapid endocytosis of interleukin 2 receptors when clathrin-coated pit endocytosis is inhibited. *J. Cell Sci.* 107:3461–3468.

47. Weidemann, T., and P. Schwille. 2013. Dual-color fluorescence cross-correlation spectroscopy with continuous laser excitation in a confocal setup. *Methods Enzymol.* 518:43–70.

48. Petrásek, Z., and P. Schwille. 2008. Precise measurement of diffusion coefficients using scanning fluorescence correlation spectroscopy. *Biophys. J.* 94:1437–1448.

49. Weidemann, T., M. Wachsmuth, …, J. Langowski. 2002. Analysis of ligand binding by two-color fluorescence cross-correlation spectroscopy. *Single Mol.* 3:49–61.

50. Bacia, K., Z. Petrasek, and P. Schwille. 2012. Correcting for spectral cross-talk in dual-color fluorescence cross-correlation spectroscopy. *ChemPhysChem.* 13:1221–1231.